RESULTS ON PROTON AND POMERON STRUCTURE FROM THE ZEUS EXPERIMENT*

For the ZEUS Collaboration presented by

A. ESKREYS

Institute of Nuclear Physics
Kawiory 26a, 30-055 Kraków, Poland

(Received April 1, 1996)

The results on the structure of proton and pomeron, obtained during the years 1993-1994 by the ZEUS experiment are presented. The proton structure function $F_2(x, Q^2)$ was measured in the deep inelastic scattering (DIS) down to x value of 3.5×10^{-5} and Q^2 down to 1.5 GeV^2 and it was found that the fast increase of this function with x decreasing persists in this region. Predictions based on DGLAP dynamics (GRV(94)) reproduce the data. The proton diffractive structure function was measured using the sample of diffractive DIS events and the comparison with QCD inspired models was made. The parton structure of pomeron is studied and the presence of the soft and hard partons is necessary to describe the data. The study of the diffractive dissociation in photoproduction revealed also the partonic nature of pomeron and allowed the rough estimation $((30-80)\%)$ of the gluon content of the pomeron.

PACS numbers: 12.38.Qk, 14.20.Dh

1. Introduction

Since the completion in 1991, the HERA collider has become a major source of information on the structure of particles such as proton, photon and pomeron. The two experiments H1 and ZEUS has played since then a decisive role in establishing the experimental evidence for these structures. The subject of this conference is just the structure of the main "bricks" of the matter and in my talk I shall present some of the results obtained in

* Presented at the Cracow Epiphany Conference on Proton Structure, Kraków, Poland, January 5–6, 1996.

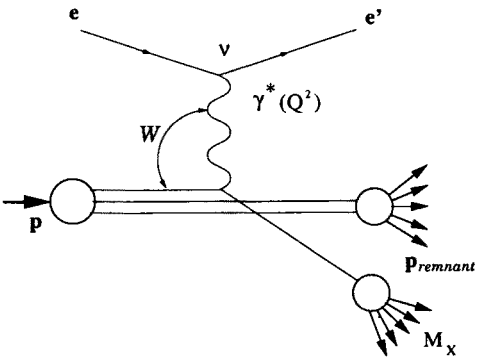

Fig. 1. Exchange diagram for DIS events. $\nu = E_e - E_{e'}$, $Q^2 = -q^2 = (e - e')^2$. $W^2 = (p+q)^2$ and p, e, e', q are the four-vectors of corresponding particles. $x_{Bj} = Q^2/2M\nu$. M_X is the mass of the hadron system coming from the fragmentation of the struck quark.

this field by the ZEUS collaboration. The presented data were collected basically during 1993–1994 running period.

HERA offers the investigation of the particle structure in the extended (compared to other experiments) ranges of Q^2 and x_{Bj} (in further denoted by x) kinematical variables — see Fig. 1 for definitions. The main idea is to probe the particle structure at the possibly small distances. Assuming that electron is a pointlike particle, by bombarding the proton with electrons one can resolve the proton structure at distances of the order of $\Delta X \sim \hbar/Q$, what at HERA means ΔX down to 10^{-16} cm. The expectation is that at these small distances a new phenomena may show up. The challenge for experimentalists is to stretch the accessible intervals of Q^2 and x as much as possible. ZEUS has explored three possibilities of such extensions:

- the installation of the new detector in the rear of the central detector, very close to the beam pipe (so called Beam Pipe Calorimeter — BPC);
- to include in the analysis the events with the radiation of bremsstrahlung photon by initial electron;
- to move the interaction vertex in the incident proton direction.

The effects on Q^2 vs x plot of the shifting of the interaction vertex and of including the measurements with the BPC are shown in Fig. 2.

For the neutral current interactions (which at HERA energies dominate over the charged current) two classes of events have to be distinguished;

- deep inelastic ep scattering (DIS) in which a large Q^2 virtual photon probes the structure of the proton and
- photoproduction reactions in which an almost real photon ($Q^2 \sim 0$) scatters on the proton or on its constituents.

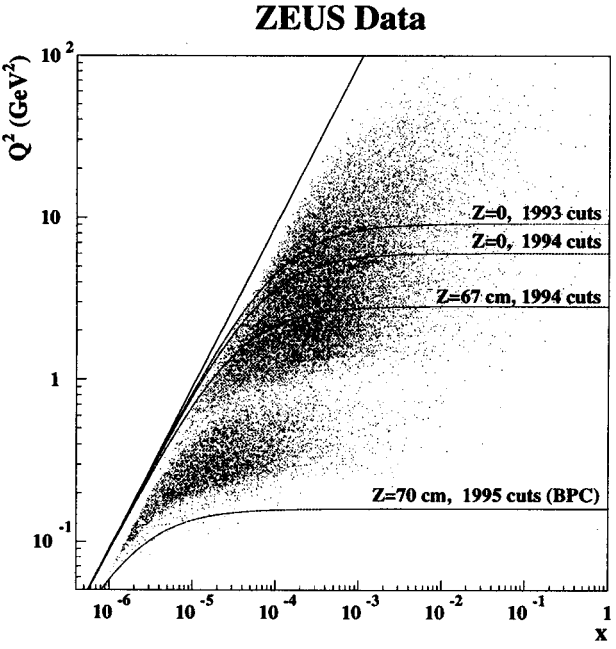

Fig. 2. Extensions of Q^2 vs x region. The full curves mark the boundaries for different conditions.

In my talk I shall concentrate on the results obtained by the ZEUS Collaboration on the structure of proton as observed in DIS events and on pomeron structure as observed in the diffractive DIS and photoproduction interactions.

2. Proton structure

2.1. Proton structure function $F_2(x, Q^2)$

The diagram (Born term) for the deep inelastic scattering is shown in Fig. 1 together with the definition of relevant quantities. Assuming that the contributions from Z^0 (δZ^0), radiative corrections (δr) and longitudinally polarized photons (δF_L) are small the one photon double differential cross section can be written in the form [1]:

$$\frac{d^2\sigma}{dxdQ^2} = \frac{2\pi\alpha^2(1+(1-y)^2)}{xQ^4} F_2(x,Q^2)(1-\delta-F_L+\delta_Z)(1+\delta_r)\,. \quad (2.1)$$

For the moderate x and Q^2 values the exchanged virtual photon sees the charged partons inside the proton and:

$$F_2(x,Q^2) = x\Sigma_q e_q^2 f_q(x,Q^2)\,, \quad (2.2)$$

where summation runs over constituent partons and $f_q(x, Q^2)$ is the parton density function. If the electron-parton scattering is pointlike F_2 should not depend on Q^2 and thus it can depend only on the dimensionless variable $x = Q^2/2M\nu$. This is known as the Bjorken scaling hypothesis [2]. In the parton model of Feynman [3] one can interpret this hypothesis as a demonstration of the elastic scattering of the virtual photon on the parton of mass m i.e. $x = Q^2/2m\nu$ and then $x = m/M$ is the fraction of proton momentum carried by the interacting parton (in the proton infinite-momentum frame).

The Bjorken scaling is not obeyed in reality. The analysis of 1993 data confirmed that one observes clear Q^2 dependence and that $F_2(x, Q^2)$ steeply rises with x decreasing and the parameterization of this function in the form:

$$F_2(x, Q^2) = (1 - x^2)^4 \left[0.35 + 0.017 x^{-(0.35+0.16 \log_{10} Q^2)}\right] \tag{2.3}$$

works very well [1].

The recent results of $F_2(x, Q^2)$ measurement for extended Q^2 vs x region are shown in Fig. 3 [4]. The earlier observations are confirmed. Two MC curves are shown in this plot GRV(94) [5] and DL [6]. While DL fails to reproduce data at small Q^2, GRV(94) based on DGLAP parton evolution [7] works remarkably well. In Fig. 4 the comparison of $F_2(x, Q^2)$ measured by different experiments is shown for $3.5 \times 10^{-5} < x < 0.1$ and $1.5\ \mathrm{GeV}^2 < Q^2 < 50000\ \mathrm{GeV}^2$. The agreement between experiments is very good and F_2 is very well described by GRV(94). It would be very interesting to check if the prediction based on BFKL evolution equations [8] also describe the data in the extended Q^2 and x intervals.

2.2. Virtual photon-proton total cross-section $\sigma_{\mathrm{tot}}^{\gamma^* p}$

For $Q^2 \neq 0$ the relation between $\sigma_{\mathrm{tot}}^{\gamma^* p}$ and $F_2(x, Q^2)$ can be written in the form [9]:

$$\sigma_{\gamma^* p}^{\mathrm{TOT}} = \frac{4\pi\ \alpha^2}{Q^4} \frac{4M^2x^2 + Q^2}{1 - x} F_2(x, Q^2)\,. \tag{2.4}$$

Remembering that $W^2 = M^2 + Q^2(1/x - 1)$, $\sigma_{\mathrm{tot}}^{\gamma^* p}$ can be studied as a function of W^2 total $\gamma * p$ c.m. energy. For small x holds the relation:

$$\sigma_{\mathrm{tot}}^{\gamma^* p} = \frac{4\pi\alpha^2}{Q^2} F_2(W, Q^2)\,. \tag{2.5}$$

Compilation of $\sigma_{\mathrm{tot}}^{\gamma^* p}$ values for different values of Q^2 from lower energy experiments [10] and from ZEUS [4] is shown in Fig. 5. The dashed line in this figure separates the two different regions:

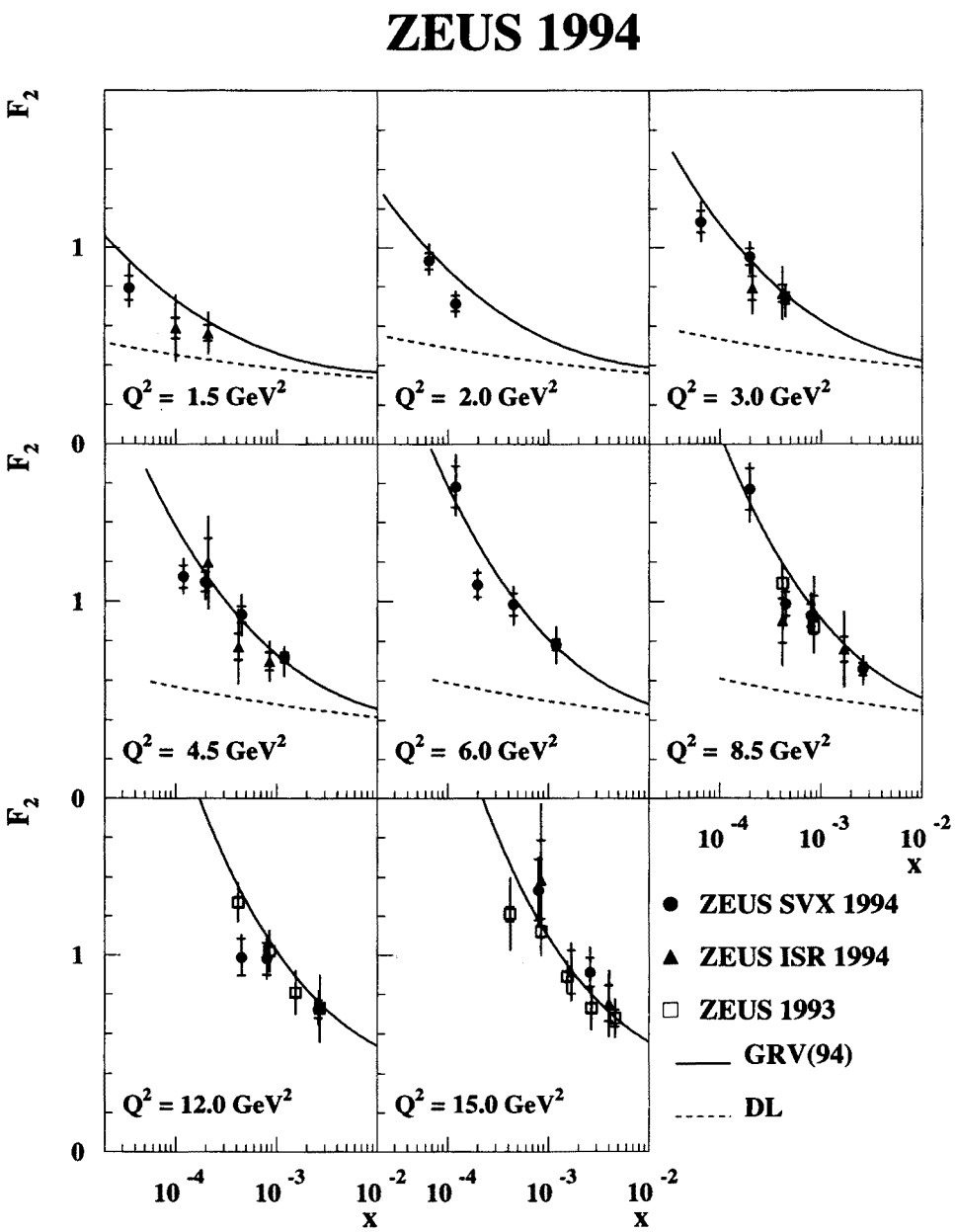

Fig. 3. Recent ZEUS results on F_2 structure function. SVX-shifted vertex, ISR — initial state radiation → see text.

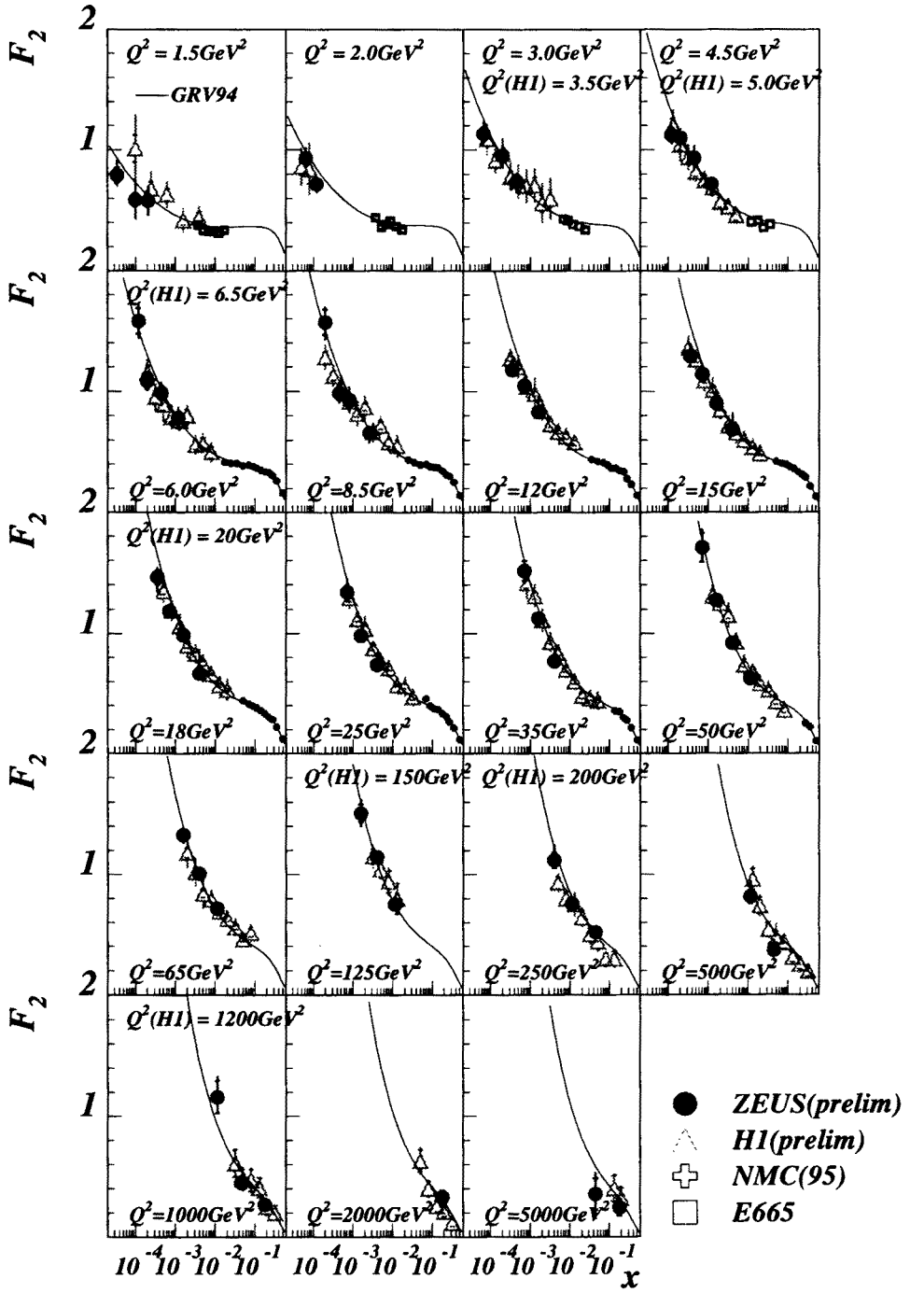

Fig. 4. Comparison of F_2 from different experiments.

- to the left of this line, the life-time of virtual photon is very short compared to the interaction time and for higher Q^2 cross section increases with W and may be reminiscent of the threshold behaviour when Q^2 approaches W^2 value;
- to the right of dashed line life-time of virtual photon exceeds the interaction time and virtual photon can be treated as physical particle.

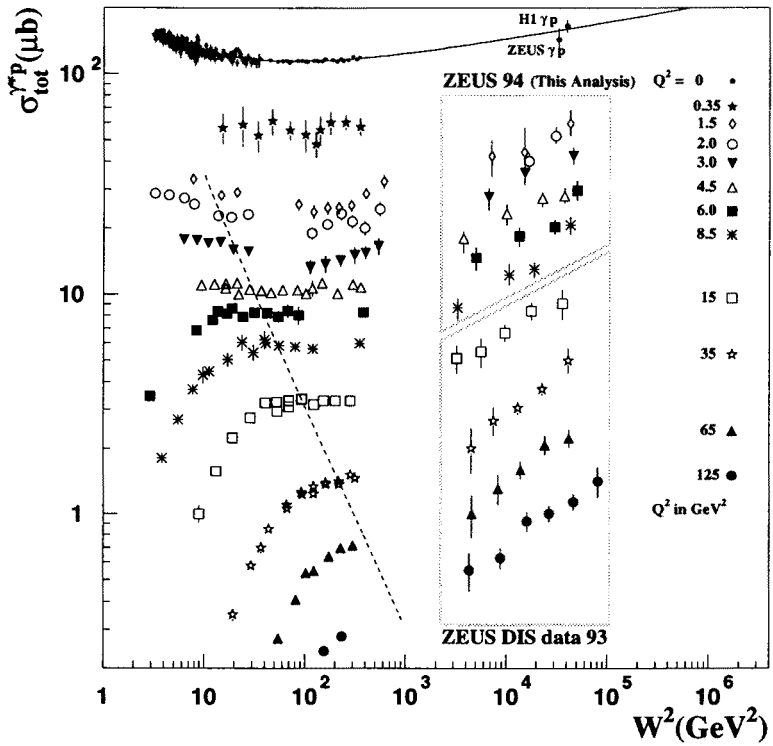

Fig. 5. Energy dependence of $\sigma_{\rm tot}^{\gamma^* p}$ for different Q^2 values.

In the region where virtual photon can be treated as physical particle the energy dependence of the cross sections at $Q^2 \neq 0$ and $Q^2 = 0$ is very different. If interpreted as due to the pomeron exchange one would have to introduce two different pomeron trajectory intercepts $\alpha(0) \sim 1.05$ for real photons and ~ 1.4 for larger Q^2. One could talk about the soft (real photoproduction) and hard pomeron (virtual photon). Where the transition between the two occurs and whether it is smooth or abrupt - this needs further investigation. The $1/Q^2$ dependence of the cross section (see 2.5) is well confirmed experimentally (see Fig. 6) [1].

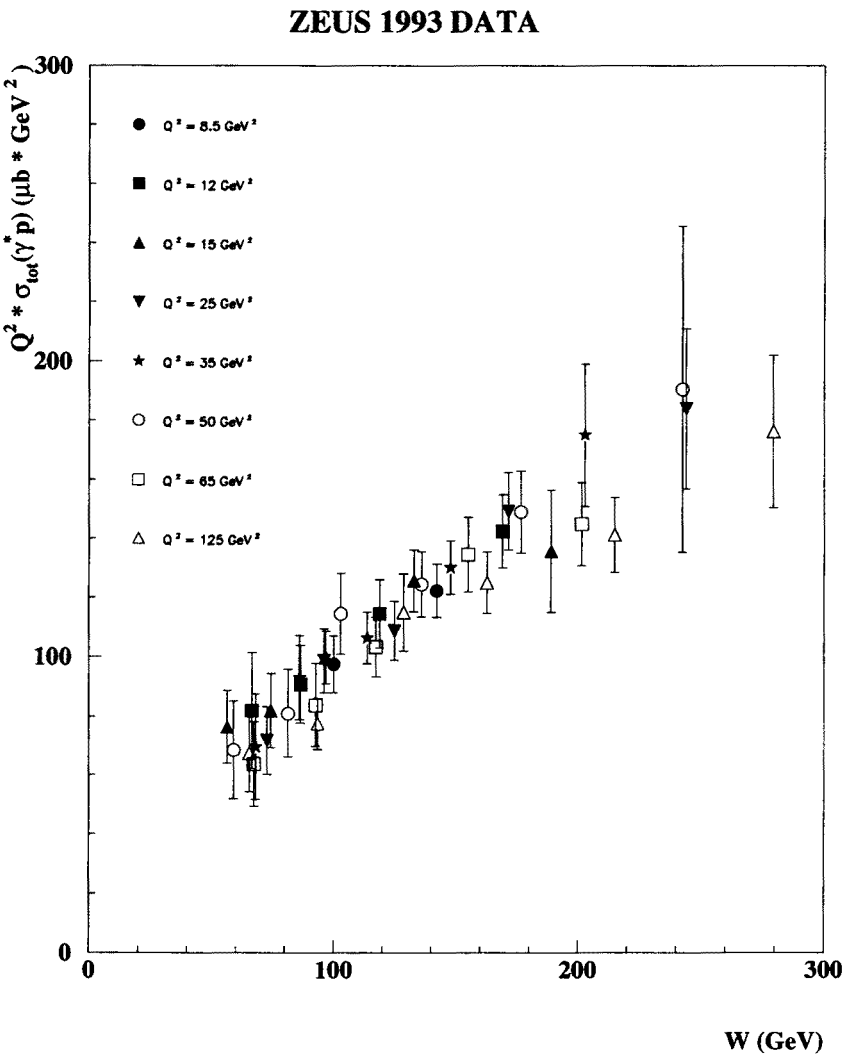

Fig. 6. Energy dependence of $Q^2 \times \sigma_{\text{tot}}^{\gamma^* p}$.

2.3. Gluon content of the proton

The Bjorken scaling violation may be interpreted as indication of the virtual photon scattering on the low energy $q - \bar{q}$ pairs coming from gluons which can be revealed at deeper penetration. The gluon momentum density can be extracted from the Q^2 dependence of F_2. The GLAP evolution equations lead to the scaling violation in the form [7]:

$$\frac{dF_2(x,Q^2)}{d\ln Q^2} = \frac{\alpha_s(Q^2)}{2\pi}\Big[\int_x^1 \frac{dz}{z}\left(\frac{x}{z}\right) P_{qq}\left(\frac{x}{z}\right) F_2(z,Q^2) + 2\Sigma_q e_q^2 \int_x^1 \frac{dz}{z}\left(\frac{x}{z}\right) P_{qg}\left(\frac{x}{z}\right) zg(z,Q^2)\Big], \tag{2.6}$$

where P_{ij} are the gluon splitting functions into ij parton pair and $zg(z,Q^2)$ is the gluon momentum density function.

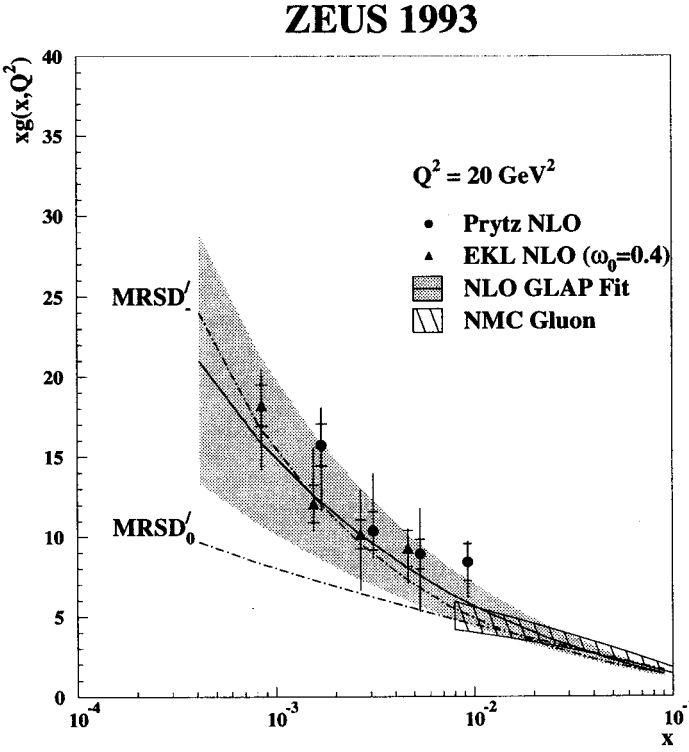

Fig. 7. Gluon momentum density function $x_g g(x_g, Q^2)$, extracted using the method of Prytz and EKL — points. Also shown is the NLO GLAP fit — full curve with shaded area reflecting the fit errors. $MRSD'_-$ and $MRSD'_0$ gluon parametrizations are shown with dotted -dashed curves.

ZEUS extracted this function [11] using the method of Prytz [12] and Ellis et al., [13] and the results are shown in Fig. 7. Both methods leads to the results which are in perfect agreement. The gluonic structure function

rises with decreasing x_g in close resemblance to the behaviour of F_2 for quarks.

In a more direct way one can extract the gluon momentum density from the vector meson production cross section, since according to Ryskin [14] and Brodsky *et al.*, [15] these cross sections are proportional to $(x_g g(x_g, Q^2))^2$.

3. Diffraction and pomeron structure

Since a long time the events with so called "large rapidity gap" — LRG were observed in the high energy hadron-hadron and lepton-hadron interactions. At HERA they are observed in both DIS and photoproduction reactions. They can be identified by filing the particle rapidities (or pseudorapidities) according to their increasing or decreasing values and looking for the large difference of rapidities of the adjacent particles. Those events in which this largest difference exceeds certain value are called LRG events. Traditionally they are believed to be the demonstration of the diffractive type dissociation of one or both colliding particles which leads at high energy to the kinematical separation of the particles coming from different initial particles. In the effect the two groups of particles are observed one to the left and the other to the right of the gap on the rapidity scale. The mechanism involved is believed to be the exchange of the pomeron trajectory. In ep collisions the gap usually occurs between the final proton or its fragments and the hadronic system coming from the dissociation of virtual photon. The diagram for such a process is shown in Fig. 8 together with definition of relevant quantities.

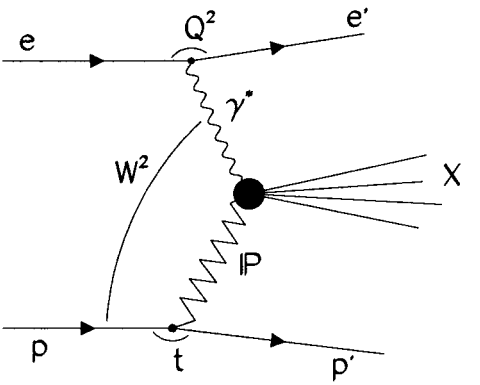

Fig. 8. Exchange diagram for DIS diffraction. Definition of variables as in Fig. 1, X is the hadron system produced in $\gamma^* \mathbb{P}$ collision and has mass M_X.

Usually the selection of the LRG events is made with the help of quantity $\eta_{\max}$ which is the maximum value of the pseudorapidity of particles in

the event (z axis of the coordinates system is defined along the incoming proton momentum and therefore the pseudorapidity is positive and maximal for a particle emitted in this direction).

3.1. Diffractive dissociation in DIS

In Fig. 9 the distributions of $\eta_{\max}$ and of M_X vs W_{DA} are shown for the DIS sample [16] [1]. In $\eta_{\max}$ distribution a clear shoulder around $\eta_{\max} = 1.5$ is observed and it is not described by the standard DIS MC [17]. The other curves in this figure correspond to MC's which include the diffractive contribution [18, 19] and they do describe the data. Using these MC's and fitting the $\eta_{\max}$ distribution one can extract the contribution of the diffractive events which amounts to $\sim (10-15)\%$ and does not depend on W, x or Q^2 [20]. It is interesting to notice that LRG events have very hard E_T distribution extending to the values of 15 GeV. The transverse energy is measured either with respect to the beam direction (E_T in ep system) or with respect to the virtual photon direction (E_T^* in $\gamma^* p$ system). In both systems for higher transverse energies practically all events have at least one jet — see Fig. 10. This could be considered as the evidence that the virtual photon undergoes hard scattering on some constituents of exchanged pomeron.

The LRG criterion is not the only one to select the diffractive dissociation events. It is also known since a long time that the mass M_X distribution is quite different in the diffractive and non-diffractive interactions. This offers another possibility to disentangle the two contributions.

In the following both approaches will be discussed for DIS sample.

3.1.1. Proton diffractive structure function

For this analysis the DIS events were selected on the basis of LRG criterion. The basic cuts were: $\eta_{\max} \leq 2.5$ and $\cos\Theta_{\mathrm{H}} \leq 0.75$ (Θ_{H} being the polar angle of the hadron system M_X). The $\gamma^* p$ diffractive cross section, integrated over t and neglecting F_L, Z^0 exchange and radiative corrections can be written in the form [20]:

$$\frac{d^3\sigma^{\mathrm{diff}}}{d\beta dQ^2 dx_{\mathbb{P}}} = \frac{2\pi\alpha}{\beta Q^4}(1+(1-y)^2)F_2^{D(3)}(\beta, Q^2, x_{\mathbb{P}}\,, \tag{3.1}$$

where $x = \beta x_{\mathbb{P}}$ and β is the fraction of the pomeron momentum carried by the interacting parton from pomeron, while $x_{\mathbb{P}}$ is the fraction of the

[1] Subscript "DA" means that these quantities were determined using the so called "double angle method" i.e. using the emission angle of the scattered electron and produced hadron system M_X

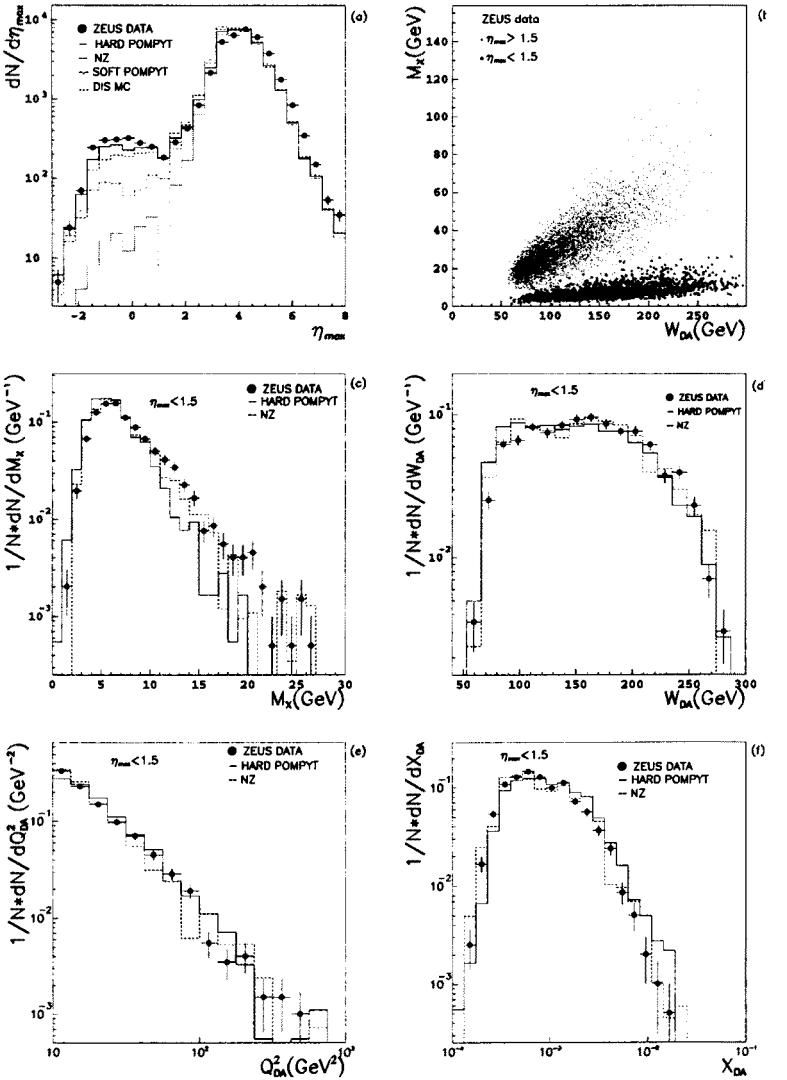

Fig. 9. Distributions of $\eta_{\max}$ and M_X vs W_{DA} for DIS events.

proton momentum carried by the pomeron. In Fig. 11. the diffractive $F_2^{D(3)}$ function is shown for different β values as function of $x_{\mathbb{P}}$ for ZEUS [20] and H1 [21] for different Q^2 values. The agreement of the two experiments is perfect and the same power law dependence of the function on $x_{\mathbb{P}}$ is observed for fixed intervals of Q^2 and β.

In the model of Ingelman and Schlein [22] the factorization of $F_2^{D(3)}$ into the flux of pomerons $f(x_{\mathbb{P}})$ and the pomeron structure function $F_2^{\mathbb{P}}(\beta, Q^2)$

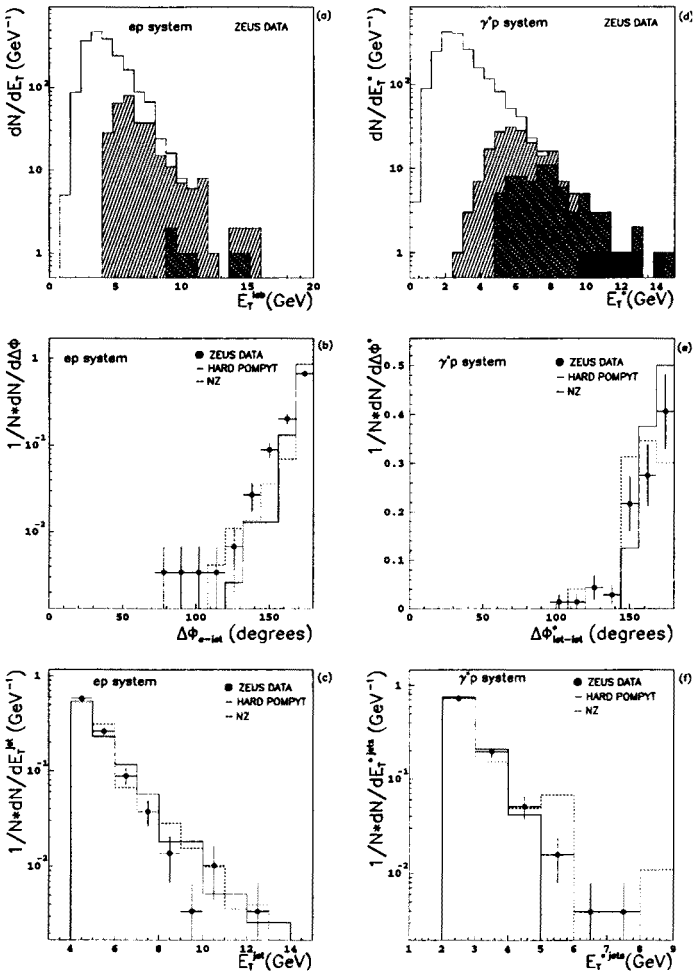

Fig. 10. E_T distribution in diffractive DIS events. Hashed histograms — $\geq$ 1-jet events, cross-hashed -$\geq$ 2-jets and full $\geq$ 3-jets.

is assumed and then:

$$F_2^{D(3)}(\beta, Q^2, x_{\mathbb{P}}) = f(x_{\mathbb{P}}) F_2^{\mathbb{P}}(\beta, Q^2) \tag{3.2}$$

and the parameterizations:

$$f(x_{\mathbb{P}}) \sim \left(\frac{1}{x_{\mathbb{P}}}\right)^{\alpha} \tag{3.3}$$

and

$$F_2^{\mathbb{P}}(\beta, Q^2) = b\big(\beta(1-\beta)\big) + \frac{c(1-\beta^2)}{2}, \tag{3.4}$$

describe the data very well. In Fig. 12 $F_2^{D(3)}$ is shown as the function of $x_{I\!P}$ together with the fit of dependence (3.3) which yields the value for $\alpha = 1.30 \pm 0.8(\text{stat})^{+0.08}_{-0.14}(\text{sys})$ independent of Q^2 and β [20].

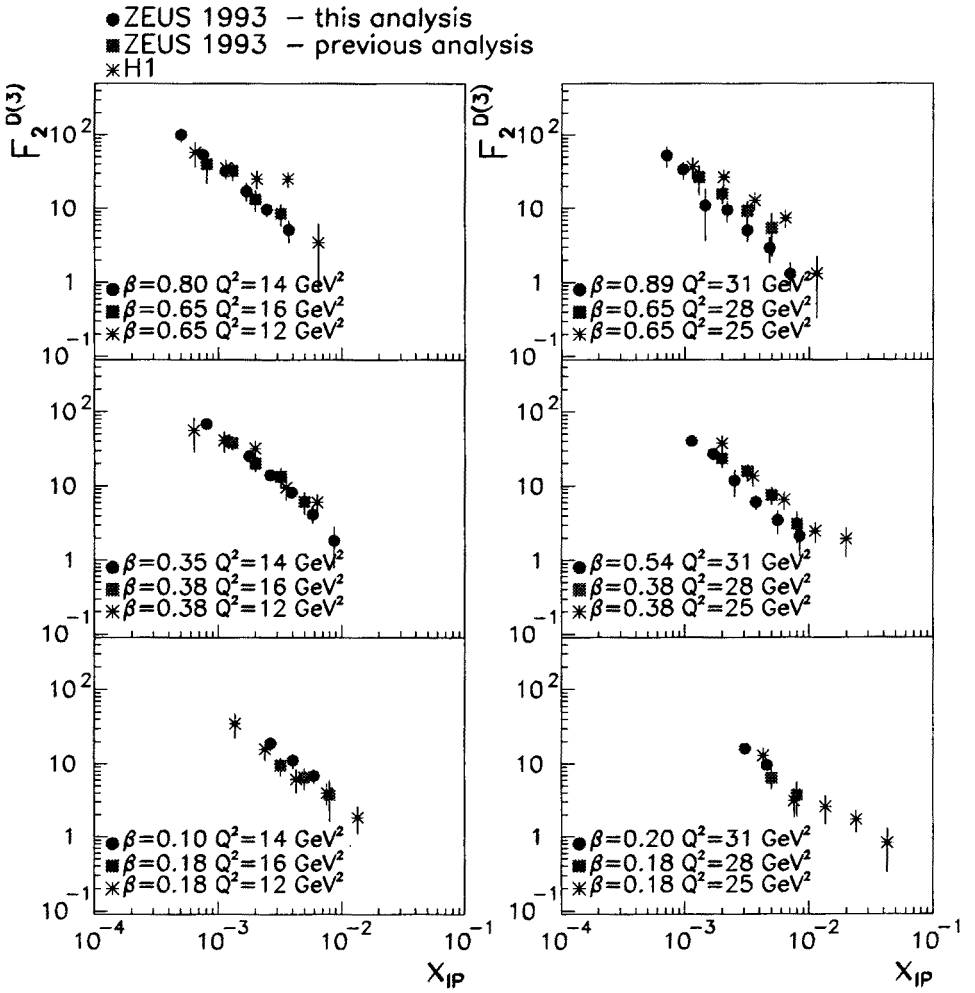

Fig. 11. $x_{I\!P}$ dependence of the proton diffractive structure function.

The integrated over $x_{I\!P}$ structure function $F_2^{D(3)}$ (denoted by $\tilde{F_2^D}$) is shown in Fig. 14. as a function of β and Q^2. No Q^2 dependence is observed The parameterization of this integrated function in the form: $b(\beta(1-\beta) + (c(1-\beta^2))/2$ works well — see Fig. 13 (full curve). For the pomeron one needs the contribution both from soft $c(1-\beta^2)$ and hard $b(\beta(1-\beta))$ partons

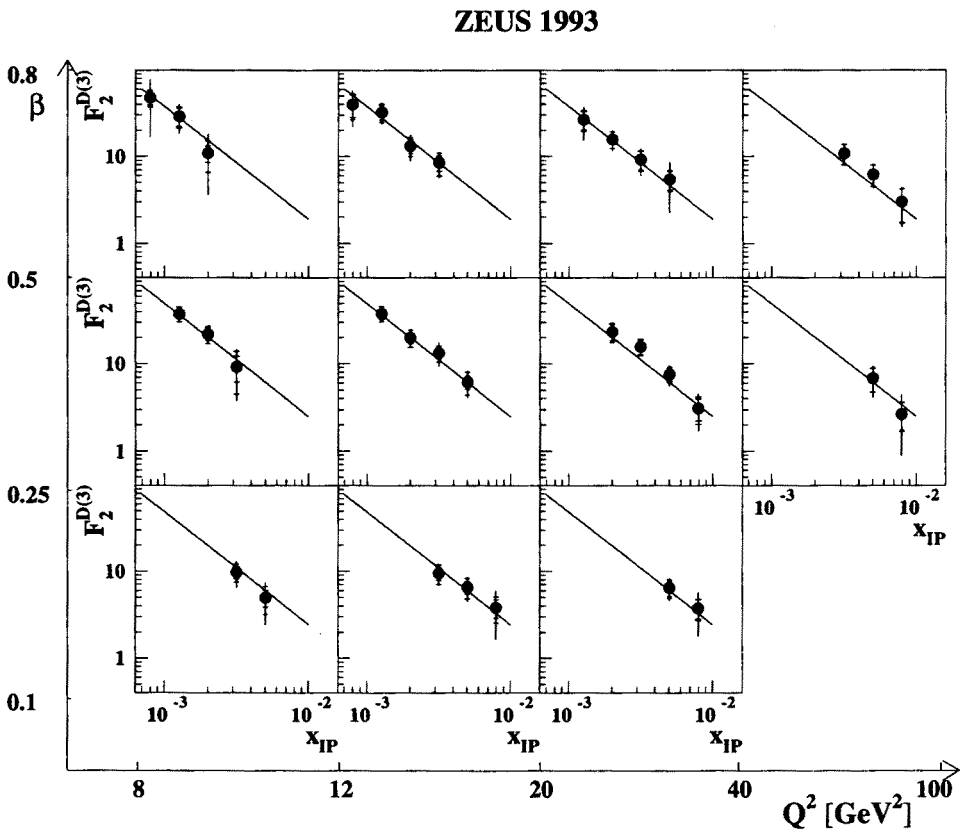

Fig. 12. Fit of formula (3.3) to the $x_{\mathbb{P}}$ dependence of the proton diffractive structure function - $F_2^{D(3)}$

(dashed curve in Fig. 13). Assuming that hard contribution is due to quarks this would mean that quarks alone are not sufficient to account for pomeron structure.

3.1.2.The mass distribution of the diffractively produced system

In the diffractive and non-diffractive interactions the M_X distributions have different shapes [23]:

- for diffraction one has:

$$\frac{dN}{d\ln M_X^2} \sim \frac{1}{(M_X^2)^n} \tag{3.5}$$

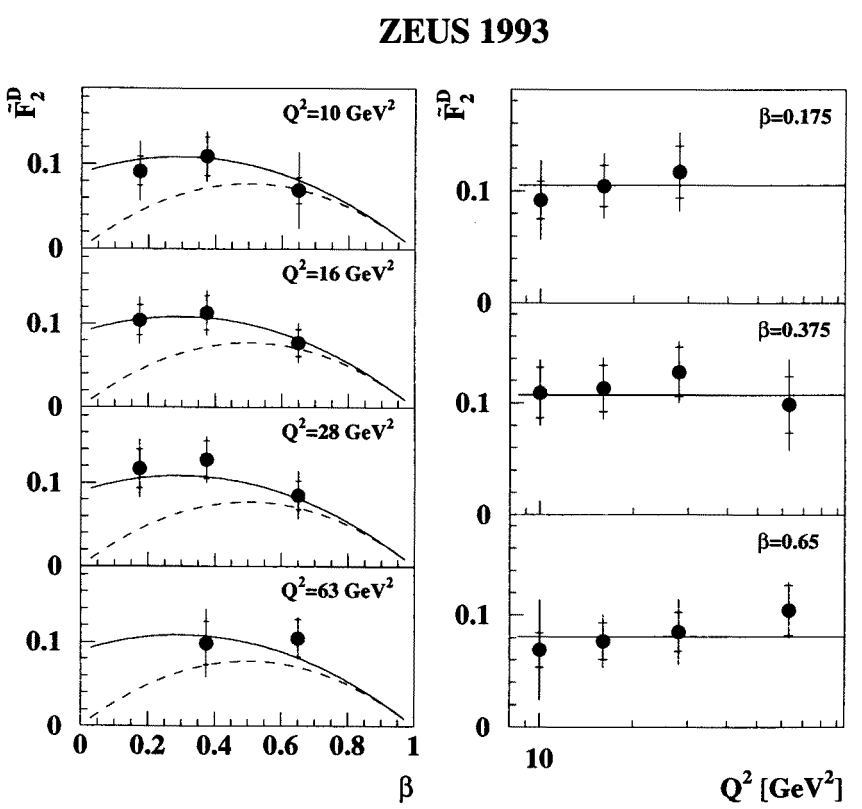

Fig. 13. β and Q^2 dependence of the integrated over $X_{\mathbb{P}}$ diffractive structure function — denoted by $\tilde{F}_2^D$.

- while for non-diffraction:

$$\frac{dN}{d\ln M_X^2} \sim \exp\left(b(\ln M_X^2)\right) . \tag{3.6}$$

The shape (3.5) for diffractive interactions was observed experimentally in pp interactions [24] and $n \sim 0$ was found. It is well reproduced by POMPYT [18] or Nikolajew–Zacharov [19] MC. The exponential fall-off towards smaller M_X^2 values for non-diffractive events is well reproduced by non-diffractive MC[2]. The unfolding of the true M_X^2 distribution from the

[2] This MC is based on codes listed in reference [17] and models the QCD cascade according to the colour dipole model including boson-gluon fusion — so called CDMBGF.

observed one was done with the help of these MC's. One then expects that non-diffractive contribution dominates at higher M_X^2 values while diffractive interactions are important at small M_X^2 values (see Fig. 9b). Then the procedure was to fit the high mass region with the exponential form, extrapolate the fit to the low mass region and treat this as the estimation of the non-diffractive contribution in the low mass region. After subtraction of the non-diffractive contribution one assumes that only diffractive contribution is left and then one can fit it with the formula:

$$\frac{dN^{\text{diff}}}{d\ln M_X^2} = D_1 + \frac{D_2}{M_X^2}. \tag{3.7}$$

The second term allows for contribution of other than pomeron exchanges. Using this method the contributions of the diffractive events were estimated

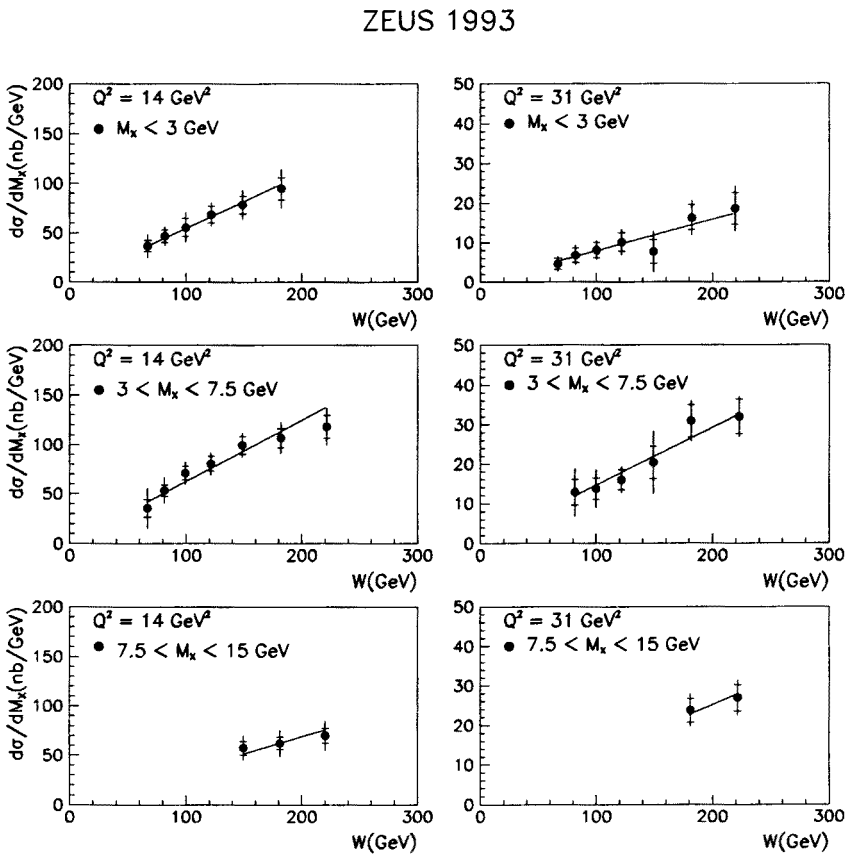

Fig. 14. Energy dependence on the diffractive $d\sigma/dM_X$ cross section.

for several W energy intervals. The calculated $d\sigma/dM_X^2$ is shown as function of W for 3 M_X^2 intervals and two Q^2 values in Fig. 14. The fit of these cross sections with the expected energy dependence for the pomeron exchange:

$$\frac{d\sigma^{\mathrm{diff}}_{\gamma^* p \to XN}(M_X, W, Q^2)}{dM_X} \sim (W^2)^{(2\bar{\alpha}_{\mathbb{P}}-2)}, \tag{3.8}$$

yields for the pomeron trajectory the value averaged over t:

$$\bar{\alpha}_{\mathbb{P}} = 1.23 \pm 0.02(\mathrm{stat}) \pm 0.04(\mathrm{sys}). \tag{3.9}$$

This value is clearly larger than the "soft" pomeron known from hadron-hadron interactions or from photoproduction of ρ mesons. This may indicate that also the hard scattering component is present in diffractive DIS mechanism.

3.2. Diffractive dissociation in photoproduction

The LRG events are observed also in photoproduction processes *i.e.* for processes with small photon virtuality $Q^2 \sim 0$. In practice this means $Q^2 \leq 4$ GeV^2. Their main demonstration is the observation of the low pseudorapidity shoulder in $\eta_{\max}$ distribution similarly as this is observed for DIS sample. Also the other features of these events are reminiscent of those in DIS — see Fig. 15 [25]. Neither $\eta_{\max}$ nor W distributions for entire sample of photoproduction sample cannot be described by non-diffractive MC like PYTHIA [26]. The MC based on the pomeron exchange mechanism like POMPYT [18] does describe small $\eta_{\max}$ shoulder and W distribution for events with $\eta_{\max} \leq 1.5$ as can be seen from Fig. 15. In this figure the expectation from purely gluonic and purely quarkonic pomeron are shown and both agree with the data for LRG ($\eta_{\max} \leq 1.5$). The LRG events have steeply falling M_X distribution and hard E_T spectrum. 8.6% of events with $E_T \geq 5$ GeV have at least one jet with $E_T^{\mathrm{jet}} \geq 4$ GeV — see Fig. 16. It is thus suggestive that also in photoproduction one deals with the hard scattering of the photon or its constituents with the colourless object inside proton.

The structure of the pomeron is still an open question, which has to be answered by experiment. One of the ways is to study the jet production. In the QCD approach the cross section for the jet production depends on the three basic factors:

- the flux of pomerons from the proton as a function of $x_{\mathbb{P}}$ and t;
- the parton densities in the pomeron;
- the matrix element for jet production.

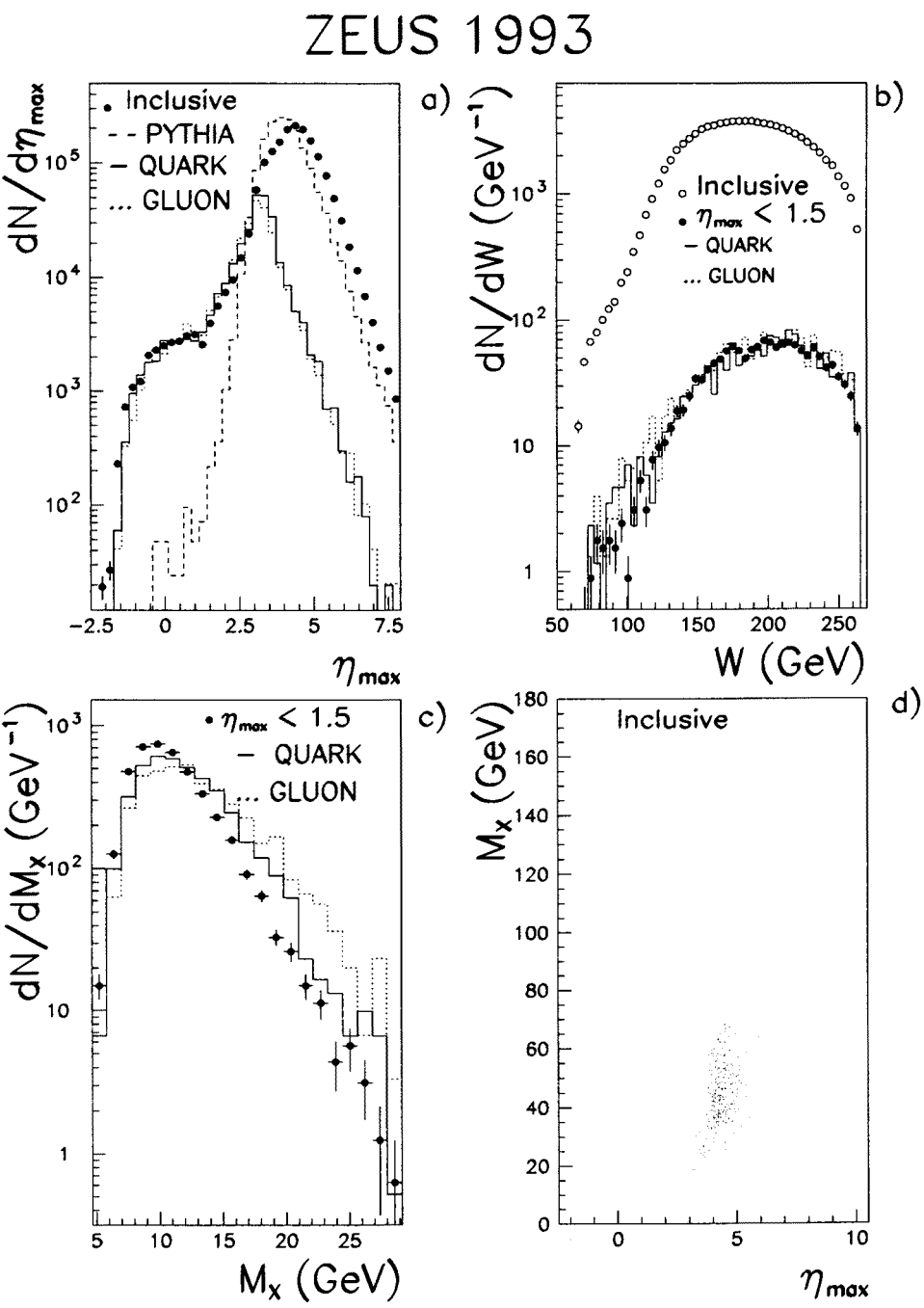

Fig. 15. $\eta_{\max}$ and W distributions for the hard photoproduction.

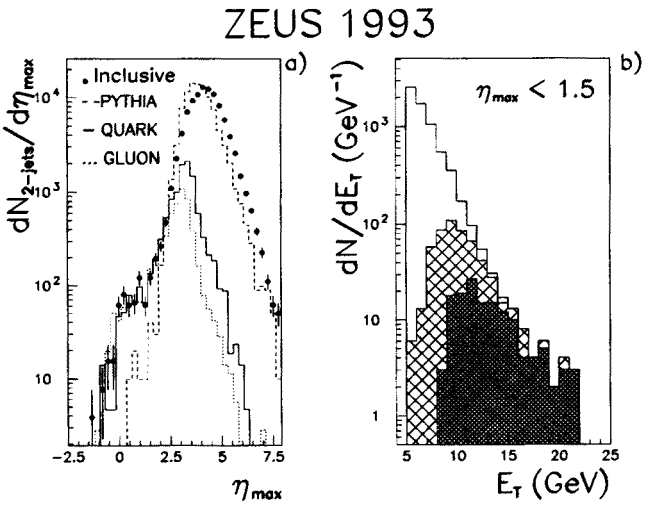

Fig. 16. a).$\eta_{\max}$ distribution for 2-jet events and b). E_T distribution for $\eta_{\max} < 1.5$ events. At least one jet — cross hashed, at least 2 jets — shaded histograms.

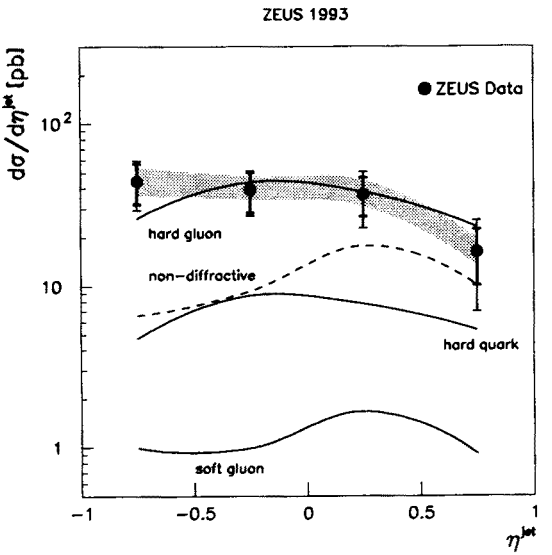

Fig. 17. Jet production cross section $d\sigma/d\eta^{\text{jet}}$ in the hard photoproduction.

It is assumed that the jet production occurs in hard interaction of the parton from pomeron with either photon (direct contribution) or with its constituent (resolved contribution). In this QCD approach the jet cross section is sensitive to the assumed parton density in the pomeron.

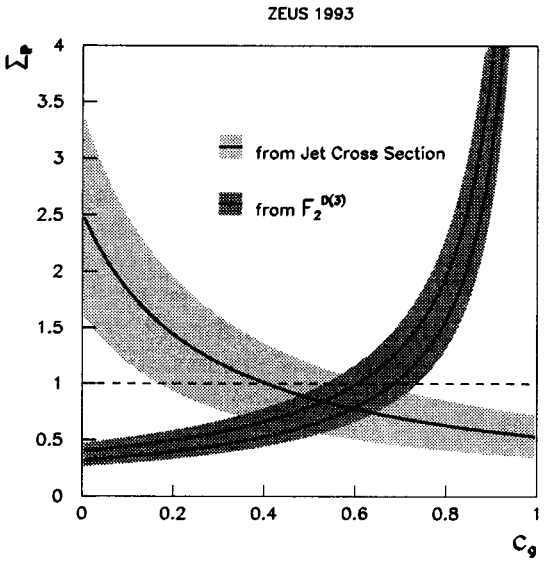

Fig. 18. Pomeron momentum sum $\Sigma_{I\!P}$ as a function of the fraction of gluons c_g.

The sample of events selected for the jet cross section analysis [27] are the LRG events with $\eta_{\max} \leq 1.8$ and $Q^2 < 4$ GeV^2 with median $Q^2 = 10^{-3}$ GeV^2. The jets were required to have transverse energy larger than 8 GeV. The jet production cross section as a function of jet pseudorapidity $d\sigma/d\eta^{\text{jet}}$ is shown in Fig. 17 together with non-diffractive PYTHIA and diffractive POMPYT MC predictions assuming different forms of the parton distributions inside pomeron. Three types of the parton densities in pomeron were considered:

- hard gluon — $\beta f_{g/I\!P} = 6(\beta(1-\beta)$;
- soft gluon — $\beta f_{g/I\!P} = 6(1-\beta)^2$;
- and hard quark — $\beta f_{q/I\!P} = (6/4)\beta(1-\beta)$.

β is the fraction of the pomeron momentum carried by the constituent parton. The densities are normalized in such a way that they satisfy

$$\int_0^1 d\beta \Sigma_i \beta f_{i/I\!P(\beta)} = 1\,,$$

for the considered partons. It is clear from the figure that the shape predicted for non-diffractive production is excluded as well as diffractive soft gluon. Both diffractive hard gluon and hard quark have shapes very similar to the data but they differ in magnitude and the hard gluon fits the data best.

An interesting exercise is shown in Fig. 18, where the results obtained in the jet production analysis and the proton diffractive structure function analysis are combined. On one hand the integral of the structure function $F_2^{D(3)}(\beta, x_{I\!P}, Q^2)$ over β and $x_{I\!P}$ is proportional to the quarks momentum sum Σ_{IPq} and assuming that the fraction of gluons in pomeron is c_g the pomeron momentum sum is $\Sigma_{IPq} = \Sigma_{I\!P}(1 - c_g)$ and it can be calculated for each c_g value. On the other hand releasing the condition $\Sigma_{I\!P} = 1$ and assuming hard gluon c_g and hard quark $(1 - c_q)$ contributions only, one can calculate $\Sigma_{I\!P}$ from the POMPYT fit to the jet production cross section for each c_g value. The results are shown in Fig. 18. The shaded bands in this figure correspond to the experimental uncertainties. The two bands overlap in the region of $0.4 < c_g < 0.7$ and $\Sigma_{I\!P} \sim 1$ indicating a substantial fraction of gluons in the pomeron.

4. Conclusions

The proton structure function $F_2(x, Q^2)$ has been measured by the ZEUS experiment using the deep inelastic scattering sample of events for Q^2 values down to 1.5 GeV^2 and x down to 3.5×10^{-5}. The rise of this function with decreasing x value is persistent for the entire studied range of x and Q^2. The data are well reproduced by the perturbative QCD calculation based on DGLAP evolution equations — GRV(94) model and agree very well with H1 and lower energy fixed target experiments. For low Q^2 values Donnachie–Landshoff predictions based on the Regge type approach are excluded.

For small x values $F_2(x, Q^2)$ can be related to the total $\gamma^* p$ cross section — $\sigma_{\rm tot}^{\gamma^* p}$ and studied as the function of energy W (c.m. energy for $\gamma^* p$ system). The energy dependence of this cross section for $Q^2 \geq 2$ GeV^2 is much stronger than for the real photoproduction. In the Regge type approach this indicates that the pomeron intercept $\alpha_{I\!P}(0)$ is for this higher Q^2 higher than that for real photoproduction and found in earlier hadron-hadron studies.

The gluon momentum density function in the proton has been extracted from the Q^2 dependence of $F_2(x, Q^2)$ and it is found that it rises fast with decreasing gluon momentum in close resemblance to the quark momentum density function.

A sizable fraction of events of the deep inelastic scattering is of diffractive type i.e. the large rapidity gap (LRG) is observed for them. In high E_T events the jet production is observed, indicating that one deals with the hard scattering. Using these events the diffractive proton structure function $F_2^{D(3)}(x_{I\!P}, \beta, Q^2)$ was measured. Assuming that the mechanism involved is the pomeron exchange, in the perturbative QCD this function factorizes into

the pomeron structure function $F_2^{\mathbb{P}}(\beta, Q^2)$ and the flux of the pomerons in the proton $f(x_{\mathbb{P}})$. The pomeron flux can be parameterized as the power function of $x_{\mathbb{P}}$ while the pomeron structure function depends on its constituent partons densities. The distributions of kinematic variables for these events are well described by POMPYT or Nikolajew–Zacharow MC's. In POMPYT both the soft (mainly gluons) and hard (mainly quarks) contributions to the parton density have to be assumed. Only hard contribution is not sufficient to describe the data.

Study of the mass of hadronic system (M_X) produced in DIS reveals the contributions from both the diffractive and the non-diffractive mechanisms. M_X distributions are quite different for diffractive and non-diffractive interactions. This allows the extraction of the diffractive contribution and calculation of the diffractive cross section, for different intervals of W. W dependence of these cross sections is well described by $\sim (W^2)^{(2\bar{\alpha}_{\mathbb{P}}-2)}$ and fits to the data yield $\bar{\alpha}_{\mathbb{P}} = 1.23 \pm 0.02(\text{stat}) \pm 0.049(\text{sys})$. This value averaged over t is much higher than that for "soft" pomeron known from the hadron-hadron interactions.

LRG events are observed also in the photoproduction ($Q^2 < 4\ \text{GeV}^2$ and median $Q^2 = 10^{-3}\ \text{GeV}^2$). Again for high E_T events the jet production is observed and they can be interpreted as due to the hard scattering of quasi-real photon (direct contribution) or its constituent (resolved contribution) with the partons inside pomeron. In the pertubative QCD the jet production cross section depends on three essential factors: the flux of pomerons in the proton, the parton density in the pomeron and the matrix element of hard interaction. Copmarison of the POMPYT with the data shows that one needs the hard parton distributions inside pomeron, the best description is obtained assuming the hard gluons.

Combining the results obtained in the study of diffraction in DIS (on proton diffractive structure function) and in the study of diffraction in photoproduction one is able to estimate the overall gluon fraction in pomeron and the result is that gluons carry between 30% and 80% of the pomeron momentum.

REFERENCES

[1] ZEUS Collab., M. Derrick *et al.*, *Z. Phys.* **C65**, 379 (1995).
[2] J.D. Bjorken, *Phys. Rev.* **163**, 1767 (1967).
[3] R.P. Feynman, *Phys. Rev. Lett.* **23**, 1415 (1969).
[4] ZEUS Collab., M. Derrick *et al.*, *Z. Phys.* **C69**, 607 (1996).
[5] M. Glűck, E. Reya, A. Vogt, *Z. Phys.* **C53**, 127 (1992); Dortmund DO - TH 93/27 (1993); *Phys. Lett.* **B306**, 391 (1993); *Z. Phys.* **C67**, 433 (1995).
[6] A. Donnachie, P.V. Landshoff, *Z. Phys.* **C61**, 139 (1994).

[7] V.N. Gribov, L.N. Lipatov, *Sov. Journ. Nucl. Phys.* **15**, 438, 675 (1972); G. Altarelli, G. Parisi, *Nucl. Phys.* **B126**, 298 (1977); Yu.I. Dokshitzer, *Sov. Phys. JETP* **46**, 641 (1977).
[8] E.A. Kuraev, L.N. Lipatov, V.S. Fadin, *Phys. Lett.* **B60**, 50 (1975); *Zh. E. T. F.* **72**, 377 (1977).
[9] A. Levy, DESY 95-003 (January 1995).
[10] NMC Collab., M. Arneodo *et al.*, CERN-PPE-95-138(1995); BCDMS collab., A.C.Benvenuti *et al.*, *Phys. Lett.* **B223**, 485 (1989); E665 Collab., Preliminary results presented by A.V. Kotwal at the XXX Rencontre de Moriond, QCD and High Energy Interactions, March 1995, FERMILAB-Conf. 95/046-Expt.(1995).
[11] ZEUS Collab. M.Derrick *et al.*, *Phys. Lett.* **B345**, 576 (1995).
[12] K. Prytz, *Phys. Lett.* **B311**, 286 (1993); *Phys. Lett.* **B322**, 393 (1994).
[13] R.K. Ellis, Z. Kunszt, E.M. Levin, *Nucl. Phys.* **B420**, 317 (1994).
[14] M.G. Ryskin, *Z. Phys.* **C57**, 89 (1993).
[15] S.J. Brodsky *et al.*, *Phys. Rev.* **D50**, 313 (1994).
[16] ZEUS Collab., M. Derrick *et al.*, *Phys. Lett.* **B332**, 228 (1994).
[17] HERACLES: A. Kwiatkowski, H. Spiesberger, H.J. Mőhring, Proc. of the Workshop on Physics at HERA, Vol. 3 DESY 1294 (1992); DJANGO: G.A. Schuler, H. Spiesberger, Proc. the Workshop on Physics at HERA, Vol. 3 DESY 1419 (1992); ARIADNE: Program Manuaql, L.Lőnnblad, DESY 92-046 (1992); PYTHIA: T. Sjőstrand, *Comp. Phys. Comm.* **39**, 347 (1986);
[18] POMPYT: P. Bruni, G. Ingelman, DESY 93-187; Proc. of Europhysics Conf. on HEP, Marseille 1993, p.595.
[19] N.N. Nikolaev, B.G. Zacharov, *Z. Phys.* **C53**, 331 (1992).
[20] ZEUS Collab., M. Derrick *et al.*, *Z. Phys.* **C68**, 569 (1995).
[21] H1 Collab., T. Ahmed *et al.*, *Phys. Lett.* **B348**, 681 (1995).
[22] G. Ingelman, P. Schlein, *Phys. Lett.* **152B**, 256 (1985).
[23] ZEUS Collab., M. Derrick *et al.*, Measurement of the Diffractive Cross Section in Deep Inelastic Scattering, DESY 96-018 (February 1996), accepted by *Z. Phys.*
[24] K. Goulianos, *Phys. Rep.*, **101**, 169 (1983); CDF Collab., F. Abe *et al.*, *Phys. Rev.* **D50**, 5535 (1994).
[25] ZEUS Collab., M. Derrick *et al.*, *Phys. Lett.* **B346**, 417 (1995).
[26] H.U. Bengtson, T. Sjőstrand, *Comp. Phys. Comm.* **46**, 43 (1987); T. Sjőstrand, CERN TH 6488/92.
[27] ZEUS Collab., M. Derrick *et al.*, *Phys. Lett.* **B356**, 129 (1995).